ACS APPLIED MATERIALS & INTERFACES

Research Article

www.acsami.org

Electrochemical Instability of Phosphonate-Derivatized, Ruthenium(III) Polypyridyl Complexes on Metal Oxide Surfaces

Jacob T. Hyde,[†] Kenneth Hanson,[‡,§] Aaron K. Vannucci,[‡,∥] Alexander M. Lapides,[‡] Leila Alibabaei,[‡] Michael R. Norris,[‡] Thomas J. Meyer,[‡] and Daniel P. Harrison*[,†]

[†]Department of Chemistry, Virginia Military Institute, Lexington, Virginia 24450, United States

[‡]Department of Chemistry, University of North Carolina at Chapel Hill, Chapel Hill, North Carolina 27599, United States

Supporting Information

ABSTRACT: The oxidative stability of the molecular components of dye-sensitized photoelectrosynthesis cells for solar water splitting remains to be explored systematically. We report here the results of an electrochemical study on the oxidative stability of ruthenium(II) polypyridyl complexes surface-bound to fluorine-doped tin oxide electrodes in acidic solutions and, to a lesser extent, as a function of pH and solvent with electrochemical monitoring. Desorption occurs for the Ru(II) forms of the surface-bound complexes with oxidation to Ru(III) enhancing both desorption and decomposition. Based on the results of long-term potential hold experiments with cyclic voltammetry monitoring, electrochemical oxidation to Ru(III) results in slow decomposition of the complex by 2,2′-bipyridine ligand loss and aquation and/or anation. A similar pattern of ligand loss was also observed for a known chromophore−catalyst assembly for both electrochemical water oxidation and photoelectrochemical water splitting. Our results are significant in identifying the importance of enhancing chromophore stability, or at least transient stability, in oxidized forms in order to achieve stable performance in aqueous environments in photoelectrochemical devices.

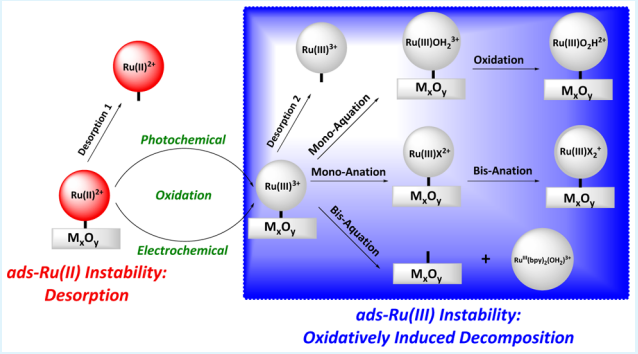

KEYWORDS: *electrochemistry, phosphonate, chromophore, ruthenium, stability, photoelectrosynthesis, dye-sensitized, interfaces*

INTRODUCTION

Small molecule dyes/chromophores on the surfaces of nanocrystalline metal oxide semiconductor electrodes, typically TiO_2, provide a basis for dye-sensitized solar cells (DSSCs) and dye-sensitized photoelectrosynthesis cells (DSPECs). Ruthenium(II) polypyridyl complexes are used extensively as sensitizers owing to their high absorptivities in the visible and near-UV spectral regions, well understood photophysical properties, and reversible one-electron transfer chemistry.[1] These complexes functionalized with phosphonate/phosphonic acid groups, as in $[Ru^{II}(4,4'\text{-}((HO)_2(O)P)_2bpy)(bpy)_2]^{2+}$ (RuP^{2+}), where 4,4′-$((HO)_2(O)P)_2$bpy is 4,4′-$((HO)_2(O)P)_2$-2,2′-bipyridine and bpy is 2,2′-bipyridine, are known to bind to metal oxide surfaces in acidic aqueous solutions. Ruthenium(II) polypyridyl-aqua derivatives used in water oxidation catalysis[2−5] and chromophore−catalyst assemblies for DSPEC water splitting[6−11] have also been derivatized with phosphonate groups and bound to metal oxides in aqueous media.

As shown in Figure 1A, excitation of RuP^{2+} bound to nanocrystalline TiO_2 (TiO_2|-RuP^{2+}) gives the metal-to-ligand charge transfer (MLCT) excited state, -RuP^{2+}*, followed by electron transfer to the conduction band of TiO_2, TiO_2|-RuP^{2+} $\xrightarrow{h\nu}$ TiO_2|-RuP^{2+}* → $TiO_2(e^-)$|-RuP^{3+}. In a DSSC, the oxidized chromophore is reduced by an external redox mediator, typically I_3^-/I^-. In a water splitting DSPEC, the oxidized chromophore is reduced by a catalyst as the first step in the accumulation of four oxidative equivalents for water oxidation. Both are in competition with back electron transfer, $TiO_2(e^-)$|-RuP^{3+}→ TiO_2|-RuP^{2+}, which, on TiO_2, occurs on the micro- to millisecond time scale and limits device efficiencies.[12] In either application, -RuP^{3+} is a short-lived transient with a finite lifetime under steady state conditions.

As illustrated in Figure 1B, electrochemical oxidation of -RuP^{2+} to -RuP^{3+} on a conductive fluorine tin oxide (FTO) electrode provides a convenient means for preparing and investigating the long-term stability of the oxidized chromophore on an oxide surface. Under positive bias, the Fermi level of FTO is sufficiently positive to oxidize surface bound RuP^{2+}. Unlike with TiO_2, back electron transfer is unfavorable unless the potential is reversed and, with no other species in solution to reduce the RuP^{3+}, the generation and lifetime of RuP^{3+} can be controlled electrochemically. Additionally, the derivatized, planar-FTO electrodes offer unhindered diffusional equilibra-

Received: February 3, 2015
Accepted: April 14, 2015
Published: April 14, 2015

DOI: 10.1021/acsami.5b01000
ACS Appl. Mater. Interfaces 2015, 7, 9554−9562

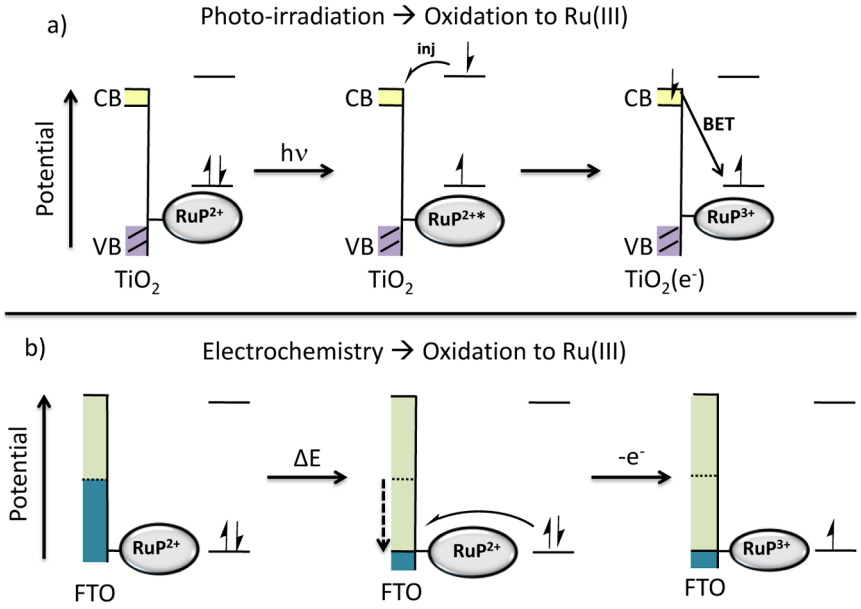

Figure 1. Comparison of formation of -RuP^{3+} by (A) excitation of -RuP^{2+} on TiO_2 and excited state electron injection (CB is conduction band, VB valence band, and BET back electron transfer) and (B) electrochemical oxidation on fluorine-doped tin oxide (FTO). The teal shading indicates the Fermi potential of the electrode.

tion with the external solution free of potential complications from intrafilm diffusion in mesoporous, nanoparticle oxide films. Typically, oxidation of surface-bound organic dyes or metal complex chromophores results in decreased stability which can greatly reduce long-term device performance. As an example, we recently reported a chromophore−catalyst based DSPEC for water splitting in which long-term performance was limited by the instability of the oxidized chromophore.[13] Understanding the origin, rates, and mechanisms of these deleterious decomposition pathways is an important element in increasing device lifetimes.

The results of a systematic investigation on the photostability of phosphonate-derivatized ruthenium(II) polypyridyl chromophores on oxide surfaces have been reported.[14,15] We report here the results of an electrochemical study on the stability of the oxidized forms of -RuP^{2+} and, to a lesser degree, the analogs -$RuP_{2\&3}^{2+}$ and -$RuCP_{1,2,\&3}^{2+}$ (Figure 2) on planar FTO electrodes. The results of a related stability study for the $1e^-$ oxidized chromophore−catalyst assembly $[(4,4'\text{-}((HO)_2(O)P)_2bpy)_2Ru_a(4\text{-Mebpy-}4'\text{-bimpy})Ru_b(tpy)(OH_2)]^{4+}$ ($[Ru_a^{II}-Ru_b^{II}-OH_2]^{4+}$, Figure 8; 4-Mebpy-4′-bimpy is 4-(methylbipyridin-4′-yl)-*N*-(benzimid)-*N*′-pyridine), and tpy is 2,2′:6′,2″-terpyridine) on nanoparticle indium doped tin oxide (*nano*-ITO) are also reported.

EXPERIMENTAL SECTION

Materials. Solvents were used as received from Fisher Scientific. Ruthenium(II) polypyridyl complexes containing three 2,2′-bipyridine or phosphonate-derivatized bpy ligands in various combinations as chloride salts were available from a previous study.[16] Following adsorption onto the electrode surfaces and submersion in the electrolyte solution (usually perchloric acid), the chloride counterions rapidly exchange for perchlorate. Structures are shown in Figure 2. For complexes containing the phosphonic acid bpy ligand functionalized at the 4- and 4′-positions, 4,4′-$((HO)_2(O)P)$-2,2′-bipyridine (4,4′-$((HO)_2(O)P)$bpy), abbreviations used are RuP^{2+} for $[Ru^{II}(4,4'\text{-}((HO)_2(O)P)bpy)(bpy)_2]^{2+}$ and RuP_2^{2+} for $[Ru^{II}(4,4'\text{-}((HO)_2(O)P)bpy)_2(bpy)]^{2+}$. For complexes with the -CH_2- methylene spacer ligands, 4,4′-$((HO)_2(O)PCH_2)$-2,2′-bipyridine, the abbreviations are

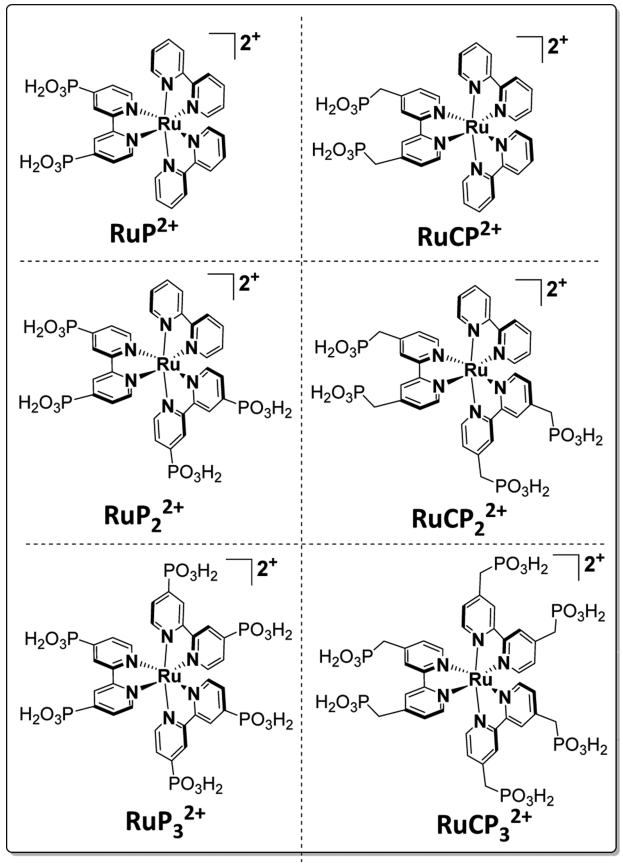

Figure 2. Structures of RuP^{2+}, RuP_2^{2+}, RuP_3^{2+}, $RuCP^{2+}$, $RuCP_2^{2+}$, and $RuCP_3^{2+}$. Chloride counterions are omitted.

$RuCP^{2+}$ for $[Ru^{II}(4,4'\text{-}((HO)_2(O)PCH_2)_2bpy)(bpy)_2]^{2+}$ and $RuCP_2^{2+}$ and $RuCP_3^{2+}$ for $[Ru^{II}(4,4'\text{-}((HO)_2(O)PCH_2)_2bpy)_2(bpy)_2]^{2+}$ and $[Ru^{II}(4,4'\text{-}((HO)_2(O)PCH_2)_2bpy)_3]^{2+}$. The chromophore−catalyst assembly $[(4,4'\text{-}((HO)_2(O)P)_2bpy)_2Ru_a(4\text{-Mebpy-}4'\text{-bimpy})Ru_b(tpy)(OH_2)]^{4+}$ (4-Mebpy-4′-bimpy is 4-(methylbipyridin-4′-yl)-

DOI: 10.1021/acsami.5b01000
ACS Appl. Mater. Interfaces 2015, 7, 9554−9562

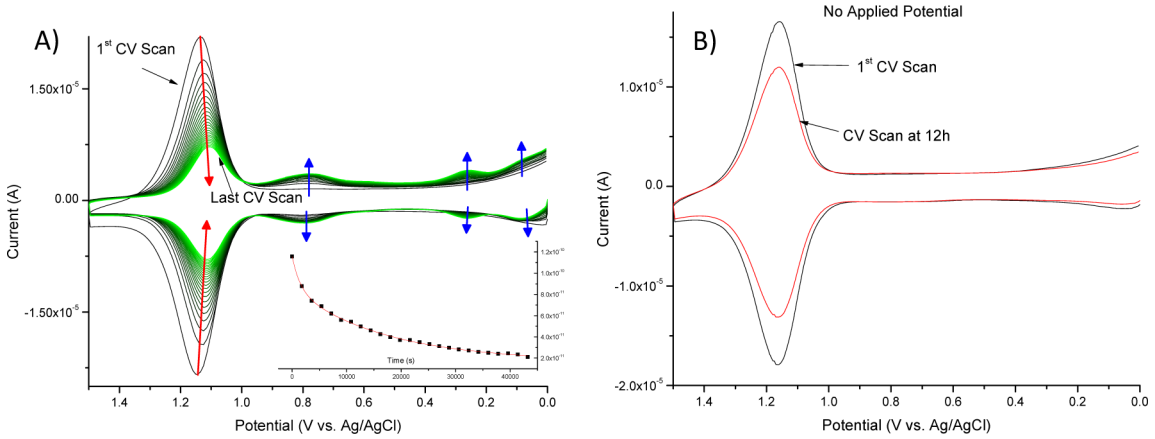

Figure 3. Cyclic voltammagrams of FTOl-RuP^{2+} in an aqueous 0.1 M $HClO_4$ solution. (A) Overlay of cyclic voltammagrams recorded every 30 min over the course of 12 h at 1.5 V vs Ag/AgCl (+0.215 V vs NHE). The red and blue arrows indicate the decrease and increase in current, respectively. The inset shows a plot of Γ (mol·cm^{-2}) vs time (s) with a biexponential fit to the data as a red curve, Supporting Information. (B) Overlay of CV's at time 0 (black trace) and at 12 h (red trace) without an applied potential.

N-(benzimid)-*N*′-pyridine); tpy is 2,2′:6′,2″-terpyridine), [Ru_a^{II}–Ru_b^{II}–OH_2]$(Cl)_4$, was synthesized as reported previously.[13]

Fluorine-doped tin oxide slides were purchased in sheets from Hartford Glass Co. Inc. and cut to individual slides of dimensions 1.0 cm wide × 3.0–4.0 cm tall. In some experiments, the slides were masked with Kapton tape to expose a surface area of 1.0 cm^2. FTO slides were cleaned by sonicating twice in isopropanol (iPrOH) for 20 min and twice in Milli-Q H_2O for 20 min and then air-dried. Nanoparticle, mesoporous indium tin oxide was prepared according to previously published procedures.[17,18]

For oxide surface loading, FTO and *nano*-ITO slides were immersed for 1 h in 0.1 mM solutions of RuP^{2+}, RuP_2^{2+}, RuP_3^{2+}, $RuCP^{2+}$, $RuCP_2^{2+}$, $RuCP_3^{2+}$, or [Ru_a^{II}–Ru_b^{II}–OH_2]$^{4+}$ in 0.1 M $HClO_4$. After 1 h, the slides were removed and rinsed with 0.1 M $HClO_4$ prior to electrochemical measurements. Monolayer surface loading occurred under these conditions as confirmed by cyclic voltammetry data at the beginning of the electrochemical stability protocol (described later). Solutions of the complexes were stored in the dark during loading and for long-term storage.

Electrochemistry. Electrochemical measurements were conducted with CH Instruments 760D, 660D potentiostats, or a Pine Wavedriver 10 potentiostat/galvanostat system in a three-compartment glass cell separated by medium- or fine-porosity frits to prevent interference from Cl^- leaching from the reference electrode. The reference electrode and platinum counter electrode were placed in each of the outermost compartments, while the electroactive face of the FTO slide was positioned toward the counter electrode. A RE-5B Ag/AgCl reference electrode with flexible connector (BASi model no. MF-2052) was used as the reference in aqueous solutions. Unless otherwise noted, all potentials are vs Ag/AgCl (+0.215 V vs NHE). The potential of the Ag/AgCl reference electrode was measured before and after randomly selected electrochemical measurements to determine the drift in electrode potential over a period of 13 h and was found to be <5 mV. Electrochemical experiments performed in nonaqueous solutions utilized a $Ag/AgNO_3$ reference electrode (BASI model no. MF-2062). The solution in the reference electrode was freshly prepared and exchanged between experiments and consisted of 0.01 M $AgNO_3$, 0.1 M tetra-*n*-butylammonium hexafluorophosphate, acetonitrile solution; −0.094 V vs ferrocene, $FeCp_2$.

Electrochemical Stability Protocol. An electrochemical protocol was developed for monitoring changes in the CV response of FTOl-RuP^{2+} electrodes as a function of time. The modified electrodes were placed in the central compartment of the three-compartment cell, described earlier, followed by (1) a series of 3 CV scans (0.0–1.5 V; sweep rate, 100 mV/s) were done to equilibrate the slide prior to recording the initial voltammogram and a single CV scan (0.0–1.5 V; sweep rate, 100 mV/s) was then collected as time 0 in time-dependent experiments; (2) an applied potential of 1.5 V vs Ag/AgCl was applied for 30 min; and (3) a single CV scan from 0.0 to 1.5 V at a sweep rate of 100 mV/s was recorded. The 30 min applied potential, single-cycle CV sequence was repeated 23 additional times with the total time held at 1.5 V of 12 h. When the CHI660D or CHI760D potentiostats were used, the cycling process was automated by using a macroprogram written into the software.

Surface Coverages. Surface coverages, Γ in mol/cm^2, were determined from CV measurements by using eq 1. In eq 1, n is the number of electrons transferred per redox site (moles e^-), F is the Faraday constant (96,485 C/mol), A is the area of the electrode (cm^2), and $Q_{E_{p,c}}$ is the integrated charge for the cathodic wave for the surface Ru(III/II) wave from CV measurements.

$$\Gamma = \frac{Q_{E_{p,c}}}{nFA} \tag{1}$$

Overlays of CV traces are not adjusted for current density for ease of plotting and because 100% loading was reached under the conditions used in the experiments. The percentage decrease in Γ, $\%\Gamma_d$, was calculated from the difference between the initial coverage and the coverage after a potential hold of 12 h, $\Gamma_{t_{app}=43{,}200s}$, eq 2.

$$\%\Gamma_d = \frac{(\Gamma_{t_{app}=43{,}200s} - \Gamma_{t_{app}=0s})}{\Gamma_{t_{app}=0s}} \times 100 \tag{2}$$

RESULTS AND DISCUSSION

Oxidatively Induced Surface Loss and Decomposition. Oxidatively induced changes in complexes and the assembly at an applied potential of 1.5 V vs Ag/AgCl in aqueous 0.1 M $HClO_4$ (+0.215 V vs NHE) were monitored by CV measurements over a 12 h period. CV scans were recorded every 30 min. The applied potential was held 400 mV higher than $E^{\circ\prime}$ values for the surface Ru(III/II) couples to ensure complete oxidation. A typical overlay of a series of voltammograms over the course of a single experiment is shown in Figure 3A.

In Figure 3A, the oxidative and reductive waves at $E_{1/2}$ = 1.15 V are characteristic of the Ru(III/II) couple for -RuP^{2+}. After 12 h of potential hold past the -$RuP^{3+/2+}$ couple, an 82 ± 5% decrease in surface coverage, $\%\Gamma_d$, for the cathodic wave was observed suggesting either decomposition or desorption of -RuP^{2+} from the surface. The decrease in RuP^{2+} Γ (mol·cm^{-2}) with time can be seen in the Figure 1A inset. A rate constant for

DOI: 10.1021/acsami.5b01000
ACS Appl. Mater. Interfaces 2015, 7, 9554–9562

the decrease in surface coverage (k_d = (6.9 ± 1.1) × 10^{-5} mol·cm^{-2}·s^{-1}) was determined from the weighted average of a biexponential fit to the data, Supporting Information. In addition to the decrease of surface coverage for the $RuP^{3+/2+}$ wave, new, reversible waves appeared at $E_{1/2}$ = 0.79, 0.26, and 0.06 V. Integration showed that the sum of surface coverages for the new surface couples was significantly less than the original coverage leading to the conclusion that -RuP^{2+} and/or its decomposition products are lost from the surface or are no longer redox active in the potential window examined.

In the absence of an applied potential only a 36% decrease in surface coverage was observed for a FTOl-RuP^{2+} electrode immersed in aqueous 0.1 M $HClO_4$ for 12 h, and there was no evidence for the appearance of new surface couples (Figure 3B). Similarly, no new couples were observed when the electrode was held at 0 V (vs Ag/AgCl). Based on these observations, the 1.5 V applied potential accelerates decomposition and/or desorption of -RuP^{2+} from the surface.

The influence of applied potential, E_{app}, on the %Γ_d for the FTOl-$RuP^{3+/2+}$ couple over a 12 h period can be seen in Figure 4. From −0.2 to 1.1 V a consistent ∼36% decrease in Γ was observed. At an applied potential of ∼1.1 V, the %Γ_d increased to ∼85%. The increase in %Γ_d coincides with the standard reduction potential for the FTOl-$RuP^{3+/2+}$ couple ($E^{\circ\prime}$ = 1.15 V vs Ag/AgCl).

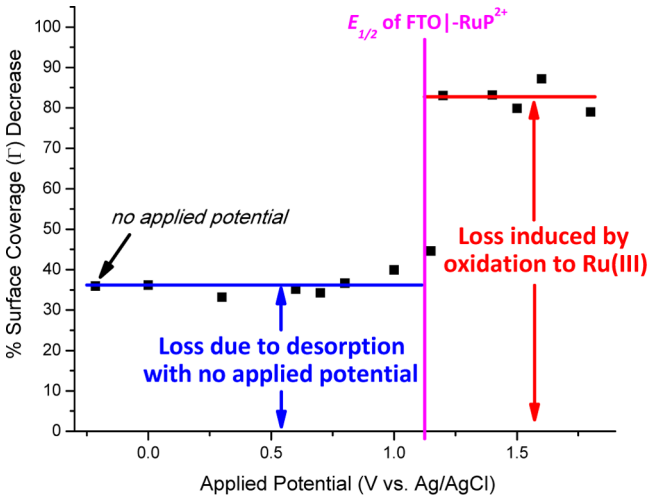

Figure 4. Percent surface coverage decrease (%Γ_d) versus applied potential (E_{app}) for FTOl-RuP^{2+} in 0.1 M $HClO_4$.

Important insights appear in these data: (1) The new waves at 0.79, 0.26, and 0.06 V (see blue arrows in Figure 3A) do not appear until E_{app} is sufficiently positive to access FTOl-RuP^{3+}. (2) Desorption and decomposition are relatively unaffected until E_{app} > $E_{1/2}$ for the FTOl-$RuP^{3+/2+}$ couple. At higher potentials both are significantly enhanced and independent of E_{app}. From these observations, slow desorption is the only process that occurs for FTOl-RuP^{2+} while oxidation to FTOl-RuP^{3+} results in decomposition products and/or accelerated desorption.

In an attempt to help elucidate the identity of the surface decomposition products responsible for new waves appearing at $E_{1/2}$ = 0.79, 0.26, and 0.06 V, a Pourbaix diagram was obtained for the postmeasurement sample (i.e., FTOl-RuP^{2+} after 12 h of potential hold at 1.5 V). $E_{1/2}$ values for the surface couples were obtained by square wave voltammetry (SWV) at pH values ranging from 1 to 7.9 at intervals of ∼0.5 units in 0.5 M $NaClO_4$ and 0.1 M aqueous buffer solutions of H_3PO_4/$H_2PO_4^-$, acetic acid/acetate, and $H_2PO_4^-$/HPO_4^{2-}. Results are shown in Figure 5A. Figure 5B shows an overlay of SWVs at various pH values above 5. Based on these results, it is possible to suggest reasonable possibilities for the decomposition products that appear on FTO surfaces.

As noted earlier, the couple at 1.15 V (black squares in Figure 5A) is consistent with the -$RuP^{3+/2+}$ couple. This couple exhibits a slight pH dependence with a slope of −9 mV/pH. A similar pH dependence has been observed for -RuP^{2+} and related surface oxide-bound complexes and has been attributed to an electric field effect.[19−23] Couple 2 at ∼0.8 V exhibits a slightly more pronounced pH dependence with a slope of −17 mV/pH. Given the potential and relatively small pH dependence similar to -RuP^{2+}, we attribute the new wave to the appearance of a κ^1-bpy perchlorato complex, -[Ru^{III}(4,4′-((HO)$_2$(O)P)$_2$bpy)(κ^2-bpy)(κ^1-bpy)(ClO_4)]$^+$. Although ClO_4^- is nominally a noncoordinating anion, the experiments were carried out in 0.1 M $HClO_4$ with a high concentration of ClO_4^- in the double layer near the electrode, and anionic ligand binding is likely more favorable for Ru(III) compared to Ru(II). For comparison, the potential for this couple is similar to that for [$Ru^{III/II}$(bpy)$_2$(py)(Cl)]$^{2+/1+}$ ($E_{1/2}$ = 0.72 V vs Ag/AgCl) and [$Ru^{III/II}$(bpy)$_2$(py)($OClO_3$)]$^{2+/1+}$ ($E_{1/2}$ = 1.05 V vs

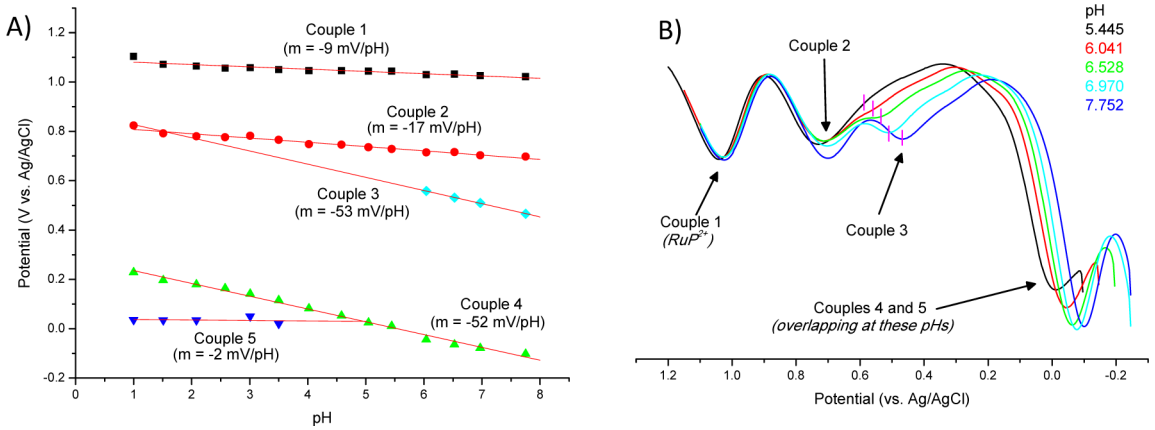

Figure 5. (A) pH-potential (Pourbaix) diagram for the couples observed after the oxidative electrochemical hold procedure for FTOl-RuP^{2+} and (B) an overlay of square wave voltammograms of the same slide as a function of pH above 5.

DOI: 10.1021/acsami.5b01000
ACS Appl. Mater. Interfaces 2015, 7, 9554−9562

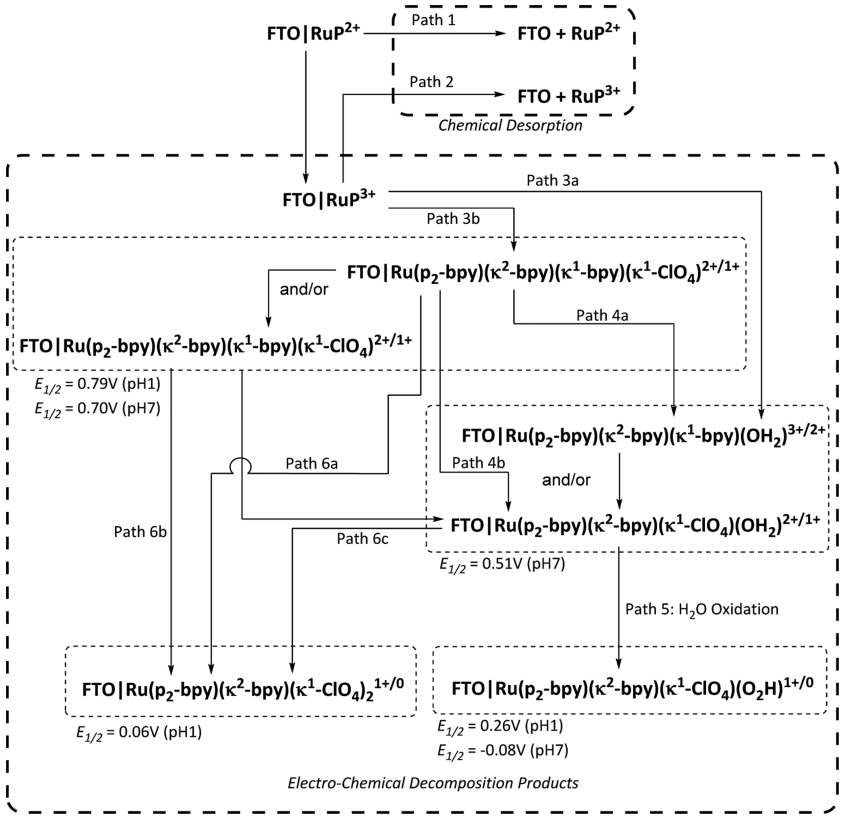

Figure 6. Simplified outline of possible desorption and decomposition pathways for FTO|-RuP^{2+} in aqueous 0.1 M $HClO_4$ at room temperature. Perchlorate counterions are omitted.

Ag/AgCl in 0.1 M (tetra-*n*-ethylammonium)(ClO_4)-MeCN).[24,25]

Couple 3 at ~0.6 V (blue diamonds in Figure 5A) exhibits a pH dependence (−53 mV/pH unit) near the expected −59 mV/pH unit dependence for a $1e^-/1H^+$ couple. The pH dependence is consistent with a Ru(III/II), $Ru^{III}-OH^{2+}/Ru^{II}-OH_2^{2+}$, couple. It may arise from the formation of $[Ru(4,4'-((HO)_2(O)P)_2bpy)(\kappa^2\text{-bpy})(\kappa^1\text{-bpy})(OH_2)]^{2+}$, with a unidentate bpy ligand, or $-[Ru(\kappa^1\text{-}4,4'-((HO)_2(O)P)_2bpy)(\kappa^2\text{-bpy})_2(OH_2)]^{2+}$, with a unidentate 4,4′-$((HO)_2(O)P)_2$bpy ligand. For comparison, the couples for $[Ru^{III/II}(bpy)_2(py)(OH_2)]^{3+/2+}$ and $[Ru^{IV}(bpy)_2(O)(OH_2)]^{2+}/[Ru^{III}(bpy)_2(OH_2)_2]^3$ appear at $E_{1/2}$ = 0.74 and 0.64 V vs Ag/AgCl, respectively. For the $[Ru^{III/II}(bpy)_2(OH_2)_2]^{3+/2+}$ couple, $E_{1/2}$ = 0.93 V (vs SSCE) below the first pK_a at ~1.5.[24,26]

At pH 1, couple 4, at 0.2 V (green triangles in Figure 5A), is pH dependent (−53 mV/pH unit). Its potential is consistent with a peroxo intermediate formed by oxidation of the aqua complex, $-[Ru(\kappa^2\text{-}4,4'-(PO_3H_2)bpy)(\kappa^2\text{-bpy})(\kappa^1\text{-bpy})(OH_2)]^{2+}$, to $Ru^V(O)^{3+}$ followed by O atom transfer to give $Ru^{III}(OOH)^{2+}$ with the pH dependence arising from the $Ru^{IV}(OOH)^{2+}/Ru^{III}(OOH)^{2+}$ couple.[2]

Couple 5 at ~0 V (blue inverted triangles in Figure 5A) is pH independent. Its potential and the absence of a pH dependence are consistent with the formation of the double anated product, $-[Ru(4,4'-(PO_3H_2)bpy)(\kappa^2\text{-bpy})(OClO_3)_2]^0$. For comparison, the $Ru(bpy)_2Cl_2^{1+/0}$ couple is 0.28 V vs Ag/AgCl in an MeCN solution with 0.1 M tetra-*n*-butylammonium hexafluorophosphate.

These observations and their interpretations are summarized in the diagram in Figure 6.

From the available data there are two distinct origins for the decrease in Γ_d for FTO|-RuP^{2+} under applied potential. Both are induced by oxidation of Ru(II) to Ru(III).

Decomposition by Ligand Dissociation. The decomposition products observed on the electrode surfaces following oxidation to -RuP^{3+} are a consequence of bpy or (4,4′-$((HO)_2(O)P)_2$bpy) dissociation from Ru(III). The electrochemical results point to a stepwise reaction with a κ^2- to κ^1-bpy chelate isomerization in the first step followed by either ClO_4^- or H_2O substituted complexes on the surface; initial κ^2- to κ^1-bpy chelate isomerization gives $-[Ru^{III}(4,4'-(\kappa^2\text{-}(HO)_2(O)P)_2bpy)(\kappa^2\text{-bpy})(\kappa^1\text{-bpy})(OClO_3)]^{2+}$, $-[Ru^{III}(\kappa^2\text{-}4,4'-((HO)_2(O)P)_2bpy)(\kappa^2\text{-bpy})(\kappa^1\text{-bpy})(OH_2)]^{3+}$, labilization of 4,4′-$((HO)_2(O)P)_2$bpy to give $-[Ru^{III}(\kappa^1\text{-}4,4'-((HO)_2(O)P)_2bpy)(\kappa^2\text{-bpy})_2(OH_2)]^{3+}$, $[Ru^{III}(\kappa^1\text{-}4,4'-((HO)_2(O)P)_2bpy)(\kappa^2\text{-bpy})_2(OClO_3)]^{2+}$, or a combination of these products. Following this initial step, complete loss of the labelized bpy ligands would produce $-[Ru^{III}(\kappa^2\text{-}4,4'-((HO)_2(O)P)_2bpy)(\kappa^2\text{-bpy})(\kappa^1\text{-}ClO_4)_2]^{1+}$, $-[Ru^{III}(\kappa^2\text{-}4,4'-((HO)_2(O)P)_2bpy)(\kappa^2\text{-bpy})(\kappa^1\text{-}ClO_4)(OH_2)]^{2+}$, $-[Ru^{III}(\kappa^2\text{-}4,4'-((HO)_2(O)P)_2bpy)(\kappa^2\text{-bpy})(OH_2)_2]^{3+}$, or a combination of these products. Attempts to obtain UV−visible absorption spectral evidence, or spectroelectrochemical data, for the proposed decomposition products utilizing mesoporous nanoparticle films of *nano*-ITO were unsuccessful due to degradation of the oxide under the potential hold conditions at E_{app} = +1.5 V (vs Ag/AgCl), requiring the exclusive use of electrochemistry to follow degradation. The base-induced ligand decomposition chemistry for $Ru^{III}(bpy)_3^{3+}$ related complexes is not a contributor in acidic solutions.[27−29]

DOI: 10.1021/acsami.5b01000
ACS Appl. Mater. Interfaces 2015, 7, 9554−9562

Surface Hydrolysis. Loss of the surface-bound complex through hydrolysis of the surface-bound phosphonates in acidic solutions is also accelerated by oxidation to Ru(III). The origin of the effect may lie in decomposition followed by desorption. Oxidatively induced hydrolysis may also be another consequence of ligand labilization following oxidation. For the surface-bound complex, substitution at a bound phosphonic acid derivatized bpy, FTO|-$[Ru^{III}(4,4'\text{-}((HO)_2(O)P)_2bpy)(bpy)_2)]^{3+}$ + $2H_2O$ → FTO|-$(4,4'\text{-}((HO)_2(O)P)_2bpy)$ + $[Ru(bpy)_2(H_2O)_2]^{2+}$, would lead to loss of the complex from the surface without a detectable Ru(III/II) response in surface voltammograms.

The initial studies on -RuP^{2+}, utilizing the same protocol, were extended to the additional set of complexes shown in Figure 2 to gain further insight into the factors that play a role oxidatively in induced decomposition/desorption. The results of these studies are summarized as follows:

(a) Ligands play an important role in both desorption and decomposition. In the series, FTO|$RuP_{1\to3}^{2+}$ and FTO|$RuCP_{1\to3}^{2+}$ (Figure 2), with a change from one to three phosphonate-derivatized bpy ligands, the rate of oxidative decomposition increases with the number of phosphonate ligands. In the series FTO|$RuP_{1\to3}^{2+}$ the phosphonate groups are electron withdrawing relative to -H as a substituent. Loss of σ electron donation by the derivatized bpy ligand to the metal destabilizes ligand binding. In the series FTO|$RuCP_{1\to3}^{2+}$, with -CH_2- spacers, the phosphonate-derivatized ligands are no longer electron withdrawing relative to -H but an additional oxidative decomposition mode appears. Although not studied in detail, evidence for this mode comes from the appearance of new, broad waves in voltammograms (Supporting Information (SI) Figure S3). The additional decomposition mode presumably arises from oxidative decomposition of the methylene spacers via O_2 (from air) or other electrochemical oxidation mechanisms.[30]

(b) Desorption is accelerated as the pH is increased from 1 to 7 as previously reported.[31,32] Decomposition and the appearance of the new aqua based couples are pH independent (see discussion in SI, accompanying Figures S4a–e and Table S2).

(c) Spontaneous decreases in Γ_d by desorption/decomposition in 0.1 M $HClO_4$ were unaffected by surface binding to indium doped tin oxide (ITO) electrodes compared to FTO, either oxygen free or by irradiation with the equivalent of 1 sun in air by a AM 1.5G solar simulator on FTO. Photoirradiation does accelerate a decrease in Γ_d on high surface area mesoporous electrodes.[14,15] Surface coverage decreases were enhanced by the mechanical motion of flowing solutions (SI Figure S5 and Table S3). The Γ_d decrease for -RuP^{2+} from FTO|-RuP^{2+} is independent of the acid added at 0.1 M for $HClO_4$, HNO_3, H_3PO_4, HOTf, or HPF_6. Decreases in surface coverage are lower with increasing concentrations of $HClO_4$ from 0.1 to 0.5 to 1.0 M. Decreases are higher as the concentration of H_2SO_4 was increased from 0.1 to 1.0 M (see discussion in SI accompanying Figure S6 and Table S4a,b).

(d) Enhanced surface stability was observed in both acetonitrile and propylene carbonate with 0.1 M added $LiClO_4$. Addition of water to both solvents enhanced a decrease in Γ_d (see discussion in SI accompanying Figure S7a–f and Table S5). The decrease in Γ for -RuP^{2+} from the electrode surface by hydrolysis in 0.1 M $HClO_4$ is inhibited by adding RuP^{2+} to the external solution at >10 μM RuP^{2+} (SI Figure S8) consistent with a solution–surface equilibrium as expected.

Chromophore–Catalyst Assembly. The chromophore–catalyst assembly, $[(4,4'\text{-}((HO)_2(O)P)_2bpy)_2Ru_a(4\text{-}Mebpy\text{-}4'\text{-}bimpy)Ru_b(tpy)(OH_2)]^{4+}$ ($[Ru_a^{II}–Ru_b^{II}–OH_2]^{4+}$), shown on an oxide surface in Figure 8, includes the $[Ru(4,4'\text{-}((HO)_2(O)P)_2bpy)_2]^{2+}$ fragment, similar to RuP_2^{2+}. Its surface loading properties and electrochemical properties, including water oxidation catalysis, were described previously.[13] As observed in the previous study, a CV of the surface-bound assembly in aqueous 0.1 M $HClO_4$ vs Ag/AgCl includes waves at 1.15, 0.99, and 0.65 V for the FTO|-$[Ru_a^{II}–Ru_b^{III}–OH_2]^{5+}$/FTO|-$[Ru_a^{II}–Ru_b^{II}–OH_2]^{4+}$, FTO|-$[Ru_a^{II}–Ru_b^{IV}{=}O]^{4+}$/FTO-$[Ru_a^{II}–Ru_b^{III}–OH_2]^{5+}$, and FTO|-$[Ru_a^{II}–Ru_b^{IV}{=}O]^{4+}$/FTO|-$[Ru_a^{III}–Ru_b^{IV}{=}O]^{5+}$ couples, respectively.[13] Oxidation at the chromophore triggers water oxidation by -$[Ru_a^{III}–Ru_b^{IV}{=}O]^{5+}$ (Figure 7, blue trace). The rate of water oxidation is enhanced by further oxidation to FTO|-$[Ru_a^{III}–Ru_b^{V}(O)]^{6+}$ at ~1.6 V which is not discernible in CVs due to catalytic water oxidation.

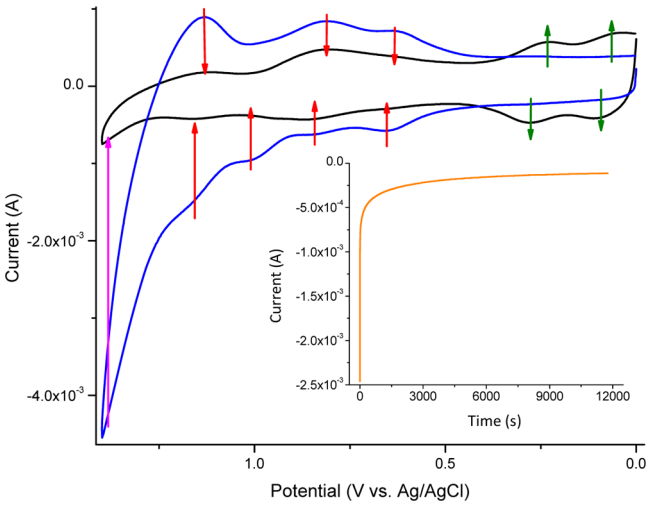

Figure 7. CVs of $[Ru_a^{II}–Ru_b^{II}–OH_2]^{4+}$ on *nano*-ITO (surface area, 1.5 cm^2) before (blue trace) and after (black trace) controlled potential electrolysis at 1.5 V for 12,000 s in aqueous 0.1 M $HClO_4$. The red arrows mark couples with decreasing currents and the green arrows the growth of new couples, and the pink arrow marks the loss of catalytic current after 1,500 s. The inset shows the current–time trace during the electrolysis.

As shown by the current–time trace in the inset in Figure 7, controlled potential electrolysis of the assembly on mesoscopic, *nano*-ITO in aqueous 0.1 M $HClO_4$ occurs with a large initial catalytic current, which decreases to a slowly diminishing steady state current after ~500 s. Based on the black trace in Figure 7 and the changes in the CV at the end of the electrolysis period, electrocatalytic water oxidation has essentially ceased after 3.3 h of electrolysis. There is also considerable loss of the assembly from the surface, and new waves for the characteristic decomposition products of FTO|-RuP_2^{3+} (SI Figure S3) appear at 0.79, 0.58, 0.24, and 0.07 V vs Ag/AgCl.

These observations are consistent with oxidatively induced hydrolysis and decomposition by ligand loss at the surface-bound chromophore. Possible decomposition pathways are illustrated in Figure 8. As shown in the figure, loss of the catalyst from the surface may occur by oxidative labilization of the bridging ligand. Decomposition of the assembly was ~87%

DOI: 10.1021/acsami.5b01000
ACS Appl. Mater. Interfaces 2015, 7, 9554–9562

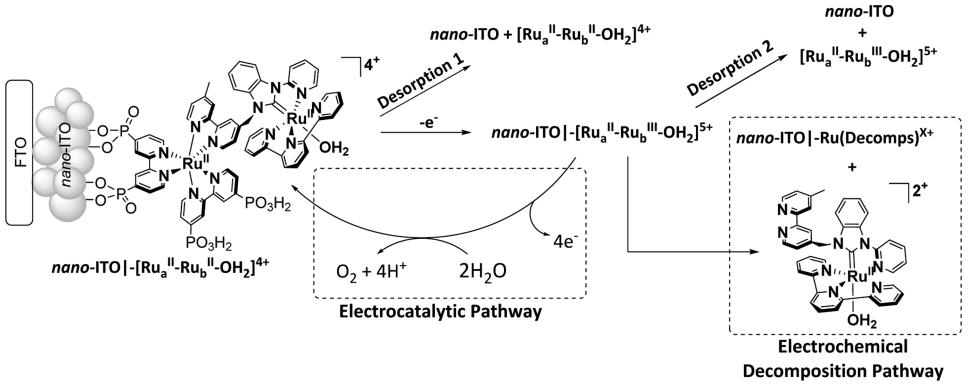

Figure 8. Simplified scheme for surface desorption/decomposition of *nano*-ITO|-$[Ru_a^{II}-Ru_b^{II}-OH_2]^{4+}$ leading to loss of water oxidation catalysis. *nano*-ITO|Ru(Decomps)X^+ in the scheme is an abbreviation for the assembly of monoanated, bis-anated, aqua-, and peroxo- decomposition products arising from -RuP_2^{3+}. Perchlorate counterions are omitted.

complete after 3.3 h, as observed by monitoring the peak current for the *nano*-ITO|-$[Ru_a^{II}-Ru_b^{IV}=O]^{5+/4+}$ couple at 1.15 V. By comparison, 69% loss of FTO|-RuP_2^{2+} occurred under the same conditions on FTO.

CONCLUSIONS

The demands on optimizing chromophores, or chromophore−catalyst assemblies, for photoanode DSPEC applications are significant. They include (1) broad absorption throughout as much of the visible and near-IR spectrum as possible; (2) an excited state or states that undergo rapid electron injection into the semiconductor oxide conduction band to give an oxidized form of the chromophore; (3) rapid, efficient oxidative activation of an integrated water oxidation catalyst; (4) long-term surface stability; and (5) chemical stability in the initial chromophore and its excited state(s) and in its oxidized form with the latter elucidated in this work.

Achieving the potentials required for water oxidation by the oxidized forms of chromophore couples typically creates a reactive entity capable of driving water oxidation. However, at these high, positive potentials, unwanted side reactions or decomposition can also occur. The results of this study highlight complications from the latter, with oxidation of surface-bound ruthenium(II) polypyridyl complexes resulting in decomposition through bpy ligand loss and aquation or anation. In an operating DSPEC under ambient sunlight a chromophore in an oxide mesoscopic film undergoes excitation at a rate of ∼2 s^{-1}. In order for water oxidation to occur, the chromophores must cycle through a four photon/four electron sequence with a solar limited rate of ∼0.5 s^{-1}. In the extreme, with the rate limiting step for water oxidation tied to the steady state presence of Ru^{III} at the chromophore, a competing decomposition reaction with a rate within a factor of 100 of the water oxidation rate would result in 1% decomposition for each photon-induced excitation cycle. Slow decomposition on this time scale resulting in decreasing photocurrents has been reported in a water splitting DSPEC with the assembly in Figure 8 with desorption from the surface occurring at an increasingly rapid rate as the pH was raised to 7.[7]

In recent results, surface stabilization toward desorption has been reported by use of atomic layer deposition (ALD) to deposit inert overlayers of Al_2O_3 or TiO_2 on top of surface-bound chromophores and catalysts.[3,33−36] In a second approach, stabilized assembly structures have been prepared by reductive electropolymerization/electroassembly formation based on vinyl-derivatized chromophores and catalysts.[37,38] Even more recently, surface stabilization has been reported by the use of hydrophobic poly(methyl methacrylate) (PMMA) polymer film overlayers.[39] However, it is clear that, in designing chromophores, coordinative stability in higher oxidation states must be considered in order for long-term stability to be achieved in active photodriven devices. Alternately, interfacial dynamics must be controlled to maximize rates of water oxidation and intraassembly electron transfer while minimizing the time spent in the oxidized state of the chromophore to avoid many of the decomposition pathways that limit the system, a strategy adopted by photosystem II in natural photosynthesis.

ASSOCIATED CONTENT

Supporting Information

Overlays of cyclic voltammagrams from electrochemical protocols under various conditions, description of surface loss dynamics and time dependence fitting of loss of -RuP^{2+}, and additional discussion and tables describing % Γ_d and surface rate constant loss data, k_d, for the series of polypyridyl complexes. This material is available free of charge via the Internet at http://pubs.acs.org.

AUTHOR INFORMATION

Corresponding Author

*E-mail: harrisondp@vmi.edu.

Present Addresses

[§]Department of Chemistry and Biochemistry, Florida State University, Tallahassee, FL 32306, USA.

[‖]Department of Chemistry and Biochemistry, University of South Carolina, Columbia, SC 29208, USA.

Notes

The authors declare no competing financial interest.

ACKNOWLEDGMENTS

D.P.H. acknowledges funding from the Virginia Military Institute (VMI) supporting the investigation of applied potentials, ligand effects on stability, and the pH-potential response of decomposed species. VMI startup funds, Equipment Trust Funds, and VMI Grants in Aid of Research funds were made available for the purchase of materials and instrumentation. L.A., K.H., M.R.N., and A.K.V. acknowledge support from the UNC EFRC: Center for Solar Fuels, an Energy Frontier Research Center funded by the U.S.

DOI: 10.1021/acsami.5b01000
ACS Appl. Mater. Interfaces 2015, 7, 9554−9562

Department of Energy, Office of Science, Office of Basic Energy Sciences under Award No. DE- SC0001011 for the study of environmental/solvent effects on surface stability. A.M.L. developed modified *nano*-ITO electrodes and acknowledges an individual fellowship from the United States Government under Grant FA9550-11-C-0028 and awarded by the Department of Defense, Air Force Office of Scientific Research, National Defense Science and Engineering Graduate (NDSEG) Fellowship, 32 CFR 168a.

REFERENCES

(1) Juris, A.; Balzani, V.; Barigelletti, F.; Campagna, S.; Belser, P.; von Zelewsky, A. Ru(II) Polypyridine Complexes: Photophysics, Photochemistry, Eletrochemistry, and Chemiluminescence. *Coord. Chem. Rev.* **1988**, *84* (0), 85−277.

(2) Chen, Z.; Concepcion, J. J.; Jurss, J. W.; Meyer, T. J. Single-Site, Catalytic Water Oxidation on Oxide Surfaces. *J. Am. Chem. Soc.* **2009**, *131* (43), 15580−15581.

(3) Vannucci, A. K.; Alibabaei, L.; Losego, M. D.; Concepcion, J. J.; Kalanyan, B.; Parsons, G. N.; Meyer, T. J. Crossing the Divide Between Homogeneous and Heterogeneous Catalysis in Water Oxidation. *Proc. Natl. Acad. Sci. U. S. A.* **2013**, *110* (52), 20918−20922.

(4) Concepcion, J. J.; Jurss, J. W.; Hoertz, P. G.; Meyer, T. J. Catalytic and Surface-Electrocatalytic Water Oxidation by Redox Mediator−Catalyst Assemblies. *Angew. Chem., Int. Ed.* **2009**, *48* (50), 9473−9476.

(5) Chen, Z.; Concepcion, J. J.; Hull, J. F.; Hoertz, P. G.; Meyer, T. J. Catalytic Water Oxidation on Derivatized *nano*-ITO. *Dalton Trans.* **2010**, *39* (30), 6950−6952.

(6) Ding, X.; Gao, Y.; Zhang, L.; Yu, Z.; Liu, J.; Sun, L. Visible Light-Driven Water Splitting in Photoelectrochemical Cells with Supramolecular Catalysts on Photoanodes. *ACS Catal.* **2014**, *4* (7), 2347−2350.

(7) Alibabaei, L.; Brennaman, M. K.; Norris, M. R.; Kalanyan, B.; Song, W.; Losego, M. D.; Concepcion, J. J.; Binstead, R. A.; Parsons, G. N.; Meyer, T. J. Solar Water Splitting in a Molecular Photoelectrochemical Cell. *Proc. Natl. Acad. Sci. U. S. A.* **2013**, *110* (50), 20008−20013.

(8) Hoertz, P. G.; Kim, Y.-I.; Youngblood, W. J.; Mallouk, T. E. Bidentate Dicarboxylate Capping Groups and Photosensitizers Control the Size of IrO_2 Nanoparticle Catalysts for Water Oxidation. *J. Phys. Chem. B* **2007**, *111* (24), 6845−6856.

(9) Swierk, J. R.; McCool, N. S.; Saunders, T. P.; Barber, G. D.; Strayer, M. E.; Vargas-Barbosa, N. M.; Mallouk, T. E. Photovoltage Effects of Sintered IrO_2 Nanoparticle Catalysts in Water-Splitting Dye-Sensitized Photoelectrochemical Cells. *J. Phys. Chem. C* **2014**, *118* (30), 17046−17053.

(10) Gao, Y.; Ding, X.; Liu, J.; Wang, L.; Lu, Z.; Li, L.; Sun, L. Visible Light Driven Water Splitting in a Molecular Device with Unprecedentedly High Photocurrent Density. *J. Am. Chem. Soc.* **2013**, *135* (11), 4219−4222.

(11) Alibabaei, L.; Sherman, B. D.; Norris, M. R.; Brennaman, M. K.; Meyer, T. J. Visible Photoelectrochemical Water Splitting into H_2 and O_2 in a Dye Sensitized Photoelectrosynthesis Cell. *Proc. Natl. Acad. Sci. U. S. A.* **2015**, DOI: 10.1073/pnas.1506111112.

(12) Durrant, J. R.; Haque, S. A.; Palomares, E. Towards Optimisation of Electron Transfer Processes in Dye Sensitised Solar Cells. *Coord. Chem. Rev.* **2004**, *248* (13−14), 1247−1257.

(13) Norris, M. R.; Concepcion, J. J.; Fang, Z.; Templeton, J. L.; Meyer, T. J. Low-Overpotential Water Oxidation by a Surface-Bound Ruthenium-Chromophore−Ruthenium−Catalyst Assembly. *Angew. Chem., Int. Ed.* **2013**, *52* (51), 13580−13583.

(14) Hanson, K.; Brennaman, M. K.; Luo, H.; Glasson, C. R. K.; Concepcion, J. J.; Song, W.; Meyer, T. J. Photostability of Phosphonate-Derivatized, Ru^{II} Polypyridyl Complexes on Metal Oxide Surfaces. *ACS Appl. Mater. Interfaces* **2012**, *4* (3), 1462−1469.

(15) Hanson, K.; Brennaman, M. K.; Ito, A.; Luo, H.; Song, W.; Parker, K. A.; Ghosh, R.; Norris, M. R.; Glasson, C. R. K.; Concepcion, J. J.; Lopez, R.; Meyer, T. J. Structure−Property Relationships in Phosphonate-Derivatized, Ru^{II} Polypyridyl Dyes on Metal Oxide Surfaces in an Aqueous Environment. *J. Phys. Chem. C* **2012**, *116* (28), 14837−14847.

(16) Norris, M. R.; Concepcion, J. J.; Glasson, C. R. K.; Fang, Z.; Lapides, A. M.; Ashford, D. L.; Templeton, J. L.; Meyer, T. J. Synthesis of Phosphonic Acid Derivatized Bipyridine Ligands and Their Ruthenium Complexes. *Inorg. Chem.* **2013**, *52* (21), 12492−12501.

(17) Farnum, B. H.; Morseth, Z. A.; Lapides, A. M.; Rieth, A. J.; Hoertz, P. G.; Brennaman, M. K.; Papanikolas, J. M.; Meyer, T. J. Photoinduced Interfacial Electron Transfer within a Mesoporous Transparent Conducting Oxide Film. *J. Am. Chem. Soc.* **2014**, *136* (6), 2208−2211.

(18) Hoertz, P. G.; Chen, Z.; Kent, C. A.; Meyer, T. J. Application of High Surface Area Tin-Doped Indium Oxide Nanoparticle Films as Transparent Conducting Electrodes. *Inorg. Chem.* **2010**, *49* (18), 8179−8181.

(19) Yan, S. G.; Hupp, J. T. Semiconductor-Based Interfacial Electron-Transfer Reactivity: Decoupling Kinetics from pH-Dependent Band Energetics in a Dye-Sensitized Titanium Dioxide/Aqueous Solution System. *J. Phys. Chem.* **1996**, *100* (17), 6867−6870.

(20) Ashford, D. L.; Song, W.; Concepcion, J. J.; Glasson, C. R. K.; Brennaman, M. K.; Norris, M. R.; Fang, Z.; Templeton, J. L.; Meyer, T. J. Photoinduced Electron Transfer in a Chromophore−Catalyst Assembly Anchored to TiO_2. *J. Am. Chem. Soc.* **2012**, *134* (46), 19189−19198.

(21) Qu, P.; Meyer, G. J. Proton-Controlled Electron Injection from Molecular Excited States to the Empty States in Nanocrystalline TiO_2. *Langmuir* **2001**, *17* (21), 6720−6728.

(22) Zaban, A.; Ferrere, S.; Gregg, B. A. Relative Energetics at the Semiconductor/Sensitizing Dye/Electrolyte Interface. *J. Phys. Chem. B* **1998**, *102* (2), 452−460.

(23) van der Vegte, E. W.; Hadziioannou, G. Acid−Base Properties and the Chemical Imaging of Surface-Bound Functional Groups Studied with Scanning Force Microscopy. *J. Phys. Chem. B* **1997**, *101* (46), 9563−9569.

(24) Moyer, B. A.; Meyer, T. J. Oxobis(2,2′-bipyridine)-pyridineruthenium(IV) Ion, $[(bpy)_2(py)Ru{:}O]^{2+}$. *J. Am. Chem. Soc.* **1978**, *100* (11), 3601−3603.

(25) Durham, B.; Walsh, J. L.; Carter, C. L.; Meyer, T. J. Synthetic Applications of Photosubstitution Reactions of Poly(pyridyl) Complexes of Ruthenium(II). *Inorg. Chem.* **1980**, *19* (4), 860−865.

(26) Dobson, J. C.; Meyer, T. J. Redox Properties and Ligand Loss Chemistry in Aqua/Hydroxo/Oxo Complexes Derived from cis- and trans-$[(bpy)_2Ru^{II}(OH_2)_2]^{2+}$. *Inorg. Chem.* **1988**, *27* (19), 3283−3291.

(27) Ghosh, P. K.; Brunschwig, B. S.; Chou, M.; Creutz, C.; Sutin, N. Thermal and Light-Induced Reduction of the Ruthenium Complex Cation $Ru(bpy)_3^{3+}$ in Aqueous Solution. *J. Am. Chem. Soc.* **1984**, *106* (17), 4772−4783.

(28) Roecker, L.; Kutner, W.; Gilbert, J. A.; Simmons, M.; Murray, R. W.; Meyer, T. J. Instability of the Oxidation Catalysts ($[(bpy)_2(py)Ru(O)]^{2+}$) and Oxo(1,10-phenanthroline)(2,2′,2″-terpyridine) Ruthenium(2+) ($[(trpy)(phen)Ru(O)]^{2+}$) in Basic Solution. *Inorg. Chem.* **1985**, *24* (23), 3784−3791.

(29) Limburg, B.; Bouwman, E.; Bonnet, S. Molecular Water Oxidation Catalysts Based on Transition Metals and Their Decomposition Pathways. *Coord. Chem. Rev.* **2012**, *256* (15−16), 1451−1467.

(30) Hanson, K.; Ashford, D. L.; Concepcion, J. J.; Binstead, R. A.; Habibi, S.; Luo, H.; Glasson, C. R. K.; Templeton, J. L.; Meyer, T. J. Sensitized Photodecomposition of Organic Bisphosphonates By Singlet Oxygen. *J. Am. Chem. Soc.* **2012**, *134* (41), 16975−16978.

(31) Trammell, S. A.; Wimbish, J. C.; Odobel, F.; Gallagher, L. A.; Narula, P. M.; Meyer, T. J. Mechanisms of Surface Electron Transfer. Proton-Coupled Electron Transfer. *J. Am. Chem. Soc.* **1998**, *120* (50), 13248−13249.

(32) Gillaizeau-Gauthier, I.; Odobel, F.; Alebbi, M.; Argazzi, R.; Costa, E.; Bignozzi, C. A.; Qu, P.; Meyer, G. J. Phosphonate-Based Bipyridine Dyes for Stable Photovoltaic Devices. *Inorg. Chem.* **2001**, *40* (23), 6073−6079.

DOI: 10.1021/acsami.5b01000
ACS Appl. Mater. Interfaces 2015, 7, 9554−9562

(33) Hanson, K.; Losego, M. D.; Kalanyan, B.; Ashford, D. L.; Parsons, G. N.; Meyer, T. J. Stabilization of $[Ru(bpy)_2(4,4'-(PO_3H_2)bpy)]^{2+}$ on Mesoporous $_{TiO_2}$ with Atomic Layer Deposition of Al_2O_3. *Chem. Mater.* **2012**, *25* (1), 3−5.
(34) Hanson, K.; Losego, M. D.; Kalanyan, B.; Parsons, G. N.; Meyer, T. J. Stabilizing Small Molecules on Metal Oxide Surfaces Using Atomic Layer Deposition. *Nano Lett.* **2013**, *13* (10), 4802−4809.
(35) Song, W.; Vannucci, A. K.; Farnum, B. H.; Lapides, A. M.; Brennaman, M. K.; Kalanyan, B.; Alibabaei, L.; Concepcion, J. J.; Losego, M. D.; Parsons, G. N.; Meyer, T. J. Visible Light Driven Benzyl Alcohol Dehydrogenation in a Dye-Sensitized Photoelectrosynthesis Cell. *J. Am. Chem. Soc.* **2014**, *136* (27), 9773−9779.
(36) Kim, D. H.; Losego, M. D.; Hanson, K.; Alibabaei, L.; Lee, K.; Meyer, T. J.; Parsons, G. N. Stabilizing Chromophore Binding on TiO_2 for Long-Term Stability of Dye-Sensitized Solar Cells Using Multicomponent Atomic Layer Deposition. *Phys. Chem. Chem. Phys.* **2014**, *16* (18), 8615−8622.
(37) Ashford, D. L.; Lapides, A. M.; Vannucci, A. K.; Hanson, K.; Torelli, D. A.; Harrison, D. P.; Templeton, J. L.; Meyer, T. J. Water Oxidation by an Electropolymerized Catalyst on Derivatized Mesoporous Metal Oxide Electrodes. *J. Am. Chem. Soc.* **2014**, *136* (18), 6578−6581.
(38) Lapides, A. M.; Ashford, D. L.; Hanson, K.; Torelli, D. A.; Templeton, J. L.; Meyer, T. J. Stabilization of a Ruthenium(II) Polypyridyl Dye on Nanocrystalline TiO_2 by an Electropolymerized Overlayer. *J. Am. Chem. Soc.* **2013**, *135* (41), 15450−15458.
(39) Wee, K.-R.; Brennaman, M. K.; Alibabaei, L.; Farnum, B. H.; Sherman, B.; Lapides, A. M.; Meyer, T. J. Stabilization of Ruthenium(II) Polypyridyl Chromophores on Nanoparticle Metal-Oxide Electrodes in Water by Hydrophobic PMMA Overlayers. *J. Am. Chem. Soc.* **2014**, *136* (39), 13514−13517.

DOI: 10.1021/acsami.5b01000
ACS Appl. Mater. Interfaces 2015, 7, 9554−9562